Materials Today Bio 24 (2024) 100884

Contents lists available at ScienceDirect

Materials Today Bio

journal homepage: www.journals.elsevier.com/materials-today-bio

Intra-articular administration of PLGA resveratrol sustained-release nanoparticles attenuates the development of rat osteoarthritis

Liwei Wei [a,1], Qingqing Pan [b,1], Junyan Teng [c], Hong Zhang [c], Na Qin [c,*]

[a] Department of Sports Medicine, Luoyang Orthopedic-Traumatological Hospital (Orthopedics Hospital of Henan Province), Luoyang, Henan, China
[b] The Third Affiliated Hospital of Xinxiang Medical University, Institutes of Health Central Plain, Clinical Medical Center of Tissue Engineering and Regeneration, Xinxiang Medical University, Xinxiang, Henan, China
[c] Bone Pharmacology Laboratory, Luoyang Orthopedic-Traumatological Hospital (Orthopedics Hospital of Henan Province), Luoyang, Henan, China

ARTICLE INFO

Keywords:
Resveratrol
Nanoparticles
Osteoarthritis
Apoptosis
Autophagy

ABSTRACT

Our previous studies have confirmed that resveratrol (RSV) can prevent the development of osteoarthritis through a variety of mechanisms, such as apoptosis inhibition, autophagy induction and SIRT 1 activation. However, the pharmaceutical application of RSV is mainly limited by its low bioavailability. Here, we designed and synthesized RSV-loaded poly (D, L-lactide-coglycolide acid) (PLGA)-nanoparticles (NPs). The average particle size, polydispersity index and positive charge of RSV-loaded PLGA NPs were 50.40 nm, 0.217 and 12.57 mV, respectively. These nanoparticles had marked encapsulation efficiency (92.35 %) and drug loading (15.1 %) for RSV. It was found that RSV-loaded PLGA NPs not only inhibited the apoptosis of chondrocytes induced by IL-1, but also rescued GAG loss in vitro. Pharmacokinetic data showed that RSV-loaded PLGA NPs demonstrated a significantly profound and prolonged concentration profile in joint tissues, with quantifiable RSV concentrations over 35 days. The therapeutic effects of RSV-loaded PLGA NPs were then examined in rat osteoarthritis models. In vitro magnetic resonance imaging results showed that RSV-loaded PLGA NPs treatment dramatically reduced both T1ρ and T2 relaxation times at 4, 8, 12 weeks during administration, implying that cartilage destruction was alleviated. Histological assessments showed that RSV-loaded PLGA NPs significantly improved osteoarthritis symptoms. Gene expression analysis revealed that osteoarthritis mediator genes were downregulated in rats treated with RSV-PLGA NPs. Mechanistic studies indicated that RSV-loaded PLGA NPs inhibit apoptosis and promote autophagy. Collectively, this study demonstrates that intra-articular delivery of RSV via PLGA NPs might be an effective therapeutic approach for osteoarthritis.

1. Introduction

Osteoarthritis is a chronic musculoskeletal disease worldwide, which affects 18 % women and 10 % men aged 60 years and older [1]. It is characterized by the gradual progression of cartilage degeneration, subchondral bone stiffness and osteophyte formation, thus resulting in joint deformity and stubborn joint pain [2]. Current therapeutic drugs, such as non-steroidal anti-inflammatory drugs (NSAIDs), analgesics, and intra-articular administration of corticosteroid or hyaluronic acid, can relieve the symptoms but not the disease progression. No drugs have been approved by the regulatory authorities so far, which require concurrent symptom improvement and structural modification [3]. Therefore, discovery of novel therapeutic agents is of great imperative for treating and preventing osteoarthritis.

Numerous in vitro and *in vivo* experiments show that resveratrol (RSV) exhibits protective effects on articular cartilage through various mechanisms, such as anti-inflammatory and anti-apoptosis, or direct regulation of different signaling pathways or active factors [4]. However, the bioavailability of RSV is relatively low, owing to its poor chemical stability, aqueous solubility and chemical stability [5,6]. There are increasing concerns about its low effectiveness caused by its low bioavailability and poor stability *in vivo* after oral ingestion. Hence, the local administration of RSV may be more suitable for clinical application than systemic administration. It has been previously reported that local

* Corresponding author. Bone Pharmacology Laboratory, Luoyang Orthopedic-Traumatological Hospital (Orthopedics Hospital of Henan Province), 82, Qiming South Road, Luoyang, 471000, Henan, China.
E-mail address: qinna2001@163.com (N. Qin).
[1] The authors contributed equally.

https://doi.org/10.1016/j.mtbio.2023.100884
Received 13 April 2023; Received in revised form 23 November 2023; Accepted 25 November 2023
Available online 12 December 2023

intra-articular administration of RSV can delay cartilage destruction in an osteoarthritis mouse model by inducing autophagy and activating SIRT1 though AMPK/mTOR signaling [7,8]. In these two experiments, RSV was administered once a week due to fear of joint infection caused by frequent intra-articular injections. However, a major limitation of these two studies is that the drug pharmacokinetics profile of RSV in knee tissues has not been analyzed. It is also uncertain whether the effective drug concentration can be maintained within the interval of administration because of the short drug half-life.

Poly (lactic-co-glycolic acid) (PLGA) nanoparticles (NPs) can be used as an effective drug carrier with high encapsulation efficiency, the excellent biocompatibility and stable release performance, therefore improving the bioavailability, solubility and stability of the drugs [9–11]. In the present study, RSV was incorporated into PLGA, and RSV-PLGA NPs were prepared. The elimination and tissue distribution of RSV-loaded PLGA NPs in the knee joint of rats were detected, and the therapeutic effects on osteoarthritis *in vivo* was evaluated.

2. Materials and methods

2.1. Preparation of RSV-PLGA-NPs

RSV-loaded PLGA NPs were prepared using the nanoprecipitation technique. *Trans*-resveratrol (MW = 228.24 g/mol) was obtained from Solarbio, China. PLGA (lactide: glycolide = 50:50, MW = 30,000–60,000 g/mol) and polyvinyl alcohol (PVA) (MW = 72,000 g/mol) were obtained from Sigma-Aldrich, USA. The main factors of microsphere formation, such as the volume ratio of oil phase and water phase, concentration of PLGA, and concentration of PVA in water phase, were investigated. RSV-loaded PLGA NPs were then prepared by the optimized solvent evaporation technique. Briefly, 50 mg of RSV and PLGA (w/w = 4:1, 2:1 and 1:1, respectively) were vortexed in acetone (2 mL) for complete solubilization to form a primary emulsion (organic phase). Next, the primary emulsion was gradually injected into PVA solution (10 mL) with varying concentrations (2.5, 5 and 7.5 mg/mL). All samples were magnetically stirred for 4 h to make acetone sufficient evaporation. After centrifugation (45,000 g, 25 min, 10 °C) (Allegra 64R, Beckman Coulter, USA), the obtained NPs were rinsed with deionized water 3 times for nanoparticle separation, followed by centrifugation to remove the excess deionized water on the upper layer. Lastly, they were frozen in a −80 °C freezer and then placed in a vacuum freeze-desiccant for lyophilization. RSV-loaded PLGA NPs were obtained and stored at 4 °C. To optimize the process, a 3^2-factorial design with 9 runs was performed according to the ratios of PLGA/RSV (Factor A) and concentration of PVA (Factor B) as independent variables. Resveratrol-free nanoparticles were similarly prepared as controls.

2.2. Characterization of RSV-PLGA-NPs

2.2.1. The particle size and zeta potential

The particle size and zeta potential of RSV-loaded PLGA NPs were detected at 25 °C using Zetasizer Nano ZS analyzer (Malvern Instruments Ltd, Malvern, UK) according to the dynamic light scattering and electrophoretic mobility principles. The freeze-dried RSV-loaded PLGA NPs were dissolved with purified water and then performed ultrasonic dispersion to obtain a solution of RSV-loaded PLGA NPs with a concentration of 0.05 % (wt/v). After 120 s of equilibrium, the sample was measured by laser Doppler velocimetry to obtain the zeta potential and particle size. The morphological characteristics of RSV-loaded PLGA NPs were observed by scanning electron microscopy (SEM). Samples were first coated with gold via a sputter-coater at 25 °C. After gold coating of the microsphere samples on a stub, their overall morphology was examined SEM (ZEISS Sigma 300).

2.2.2. Entrapment efficiency and drug loading

To detect drug encapsulation rate and load efficiency, the concentration of RSV in nanospheres was detected by HPLC. Briefly, 5 mg of lyophilized RSV-containing PLGA NPs are added with 0.5 mL of dichloromethane and vortexed to disrupt the structure of the spheroids, resulting in complete release of the drug. After adding 10 mL of methanol, centrifuge the samples at 12,000 g for 20 min at 4 °C. Then, the supernatant (20 μL) is taken into the column for determination. Calibration curve of the methanol solution using RSV (standard solution in the range of 0.5–20 μg/mL; $R^2 = 0.9961$) to calculate the RSV content in the corresponding sample. Entrapment rate = Actual DL/Theoretical DL × 100 %; DL = Actual drug content in microspheres/Total weight of lyophilized microspheres × 100 %.

2.2.2.1. HPLC method validation. According to internationally accepted guidelines ((ICH Harmonised Tripartite Guideline), the proposed HPLC procedure was validated (Fig. S1).

2.2.2.2. Linearity. A good linear relationship was obtained with six concentrations (0.5, 1.00, 5.00, 10.00, 15.00, 20.00 μg/mL) of resveratrol standards in three injections over 3 days. Each peak area vs. concentration and linearity is plotted by least squares regression analysis.

2.2.2.3. Limit of detection and limit of quantification. The signal-to-noise ratio (S/N) method was used to calculate the limit of detection (LOD) and limit of quantification (LOQ). A concentration equal to 3 is LOD, and a concentration equal to 10 is LOQ. Within 3 days, the resveratrol test solution is injected into the system in triplicate.

2.2.2.4. Precision of method. Intraday and interday precision was used, and the resveratrol test solution was injected 3 times for 3 consecutive days, and the concentration of the injected solution was determined as the low, medium, and high level of the calibration curve.

2.2.2.5. Accuracy of method. The accuracy of HPLC method was determined at 80 %, 100 % and 120 % by standard addition method. Add a known amount of resveratrol to the pre-analyzed nanoparticle sample solution and repeat 3 times per level.

2.2.2.6. Robustness of method. In order to assess the robustness of the method, different chromatographic conditions were investigated: flow rate, oven temperature and detection wavelength.

2.2.2.7. Specificity of method. The samples were subjected to stress conditions to verify molecular degradation, and the degradation of the samples was examined by changing the acid-base environment, thermal environment and light conditions.

2.2.3. Fourier-transform infrared spectroscopy of RSV-PLGA-NPs

The infrared spectra of RSV, PLGA-NPs and RSV-PLGA-NPs in the band of 4000–500 cm^{-1} were detected by infrared absorption spectrometry (Bruker, Tensor II, Germany).

2.2.4. Differential scanning calorimetry of RSV-PLGA-NPs

DSC instrumentation (Perkin Elmer, USA) was used for RSV-PLGA-NPs perform differential scanning calorimetry.

2.2.5. Degradation assay in vitro of RSV-PLGA-NPs

RSV-PLGA-NPs were dispersed in pH 7.4 and 6.4 PBS, respectively. In vitro degradation kinetics are performed at 37 °C in a shaker at 200 rpm. The pH of the sample is determined daily with a pH meter. The RSV-PLGA-NPs were then dispersed in the culture medium, the simulated body fluid was changed every day, and the lyophilized was taken out for scanning electron microscopy (SEM) at 14 and 28 days to evaluate the degradation of microspheres.

2.2.6. Release test of resveratrol from RSV-PLGA-NPs

To mimic the acidic environment of osteoarthritis and the release of drugs under normal physiological conditions, The drug release of RSV-loaded PLGA NPs was studied in PBS (pH 7.4 and pH 6.4) (contains 0.5 % Tween 80) using the dialysis bag (MW: 3500 KD) method as reported previously [12]. Approximately 6 mg of the sample was placed in a dialysis bag, which was then placed in a PBS solution. The beaker containing the dialysis bag was placed in a shaker (Yiheng, THZ-98A, China) at 37 °C and 100 rpm/min, a certain amount of dialysate was taken out every day according to the predetermined time point, and then supplemented with fresh dialysate of equal volume, and the concentration of RSV was measured by ultraviolet spectrophotometry. Briefly, we detected the absorbance value of *trans*-resveratrol containing liquids taken at different time points at 320 nm by ultraviolet spectrophotometry. Then, according to the *trans*-resveratrol concentration of 0.5, 1.00, 5.00, 10.00, 15.00, 20.00 μg/mL, the absorbance value was determined at 320 nm, and the standard curve under different pH conditions was drawn with the drug concentration as the abscissa (X) and the absorbance value (OD_{320}) as the ordinate (Y) to calculate the RSV content in the corresponding release solution.

cumulative release % = $W_0/W_1 \times 100$ %

W_0 is the total amount of RSV that had been released in PBS solution including being sampled every time point, and W_1 is the total amount of RSV encapsulated in RSV-PLGA-NPs.

2.3. Evaluation of biologic activity and cellular internalization of RSV-PLGA-NPs

2.3.1. Cytotoxicity assay

Normal human knee articular chondrocytes were cultured in α-MEM (Gibco, USA) supplemented with 10 % (v/v) FBS (Gibco, USA) and 1 % (v/v) penicillin/streptomycin (Solarbio, China) at 37 °C and 5 % CO_2. RSV-loaded PLGA NPs at different concentrations were added into the medium to evaluate its cytotoxicity on chondrocytes using the Cell Counting Kit-8. Resveratrol-free nanoparticles were used as the control. Then, RSV-PLGA-NPs (100 μg/mL) were incubated with chondrocytes for 1, 3, and 7 days after screening for suitable concentrations. As mentioned above, the CCK-8 kit was used to detect the OD value of each group of chondrocytes at 450 nm.

2.3.2. Live/dead assay

The chondrocytes were exposed to 1 μL FDA (5 mg/mL stock solution in acetone, final amount = 5 μg) and 1 μL PI (5 mg/mL stock solution in PBS; Invitrogen, USA) at 37 °C for 5 min in the darkness after rinsing 3 times with PBS. Next, all samples (100 μL) were dispensed in a 96-well black plate in triplicate and analyzed with fluorescent microscopy. Live/dead cell ratio was measured as the relative ratio of green/red fluorescence units.

2.3.3. Flow cytometry detection of apoptosis

Annexin V-FITC-PI kit (4A biotech) was utilized to examine chondrocytes apoptosis. Briefly, 1×10^5 cells were collected and suspended at 200 μL Binding Buffer. Then, 0.5 mg/mL PI (4 μL) and Annexin V-FITC solution (2 μL) were added, followed by incubation at room temperature (RT) for 15 min in the darkness. Finally, fluorescence was determined by flow cytometry.

2.3.4. Quantification of intracellular glycosaminoglycan (GAG)

Chondrocytes were then exposed to IL-1β (10 ng/mL) for 2 h, followed by treatment with RSV-loaded PLGA NPs (10 μM). The chondroprotective effects of RSV-loaded PLGA NPs were assessed by FDA/PI live/dead assay, annexin V FITC and PI assay (Clontech, CA) and DMMB assay for detecting GAG expression.

2.3.5. Cellular internalization of RSV-PLGA-NPs

After co-culture RSV-PLGA-NPs with chondrocytes for 24 h, after rinsing the excess nanoparticles with PBS, the uptake of the nanoparticles by chondrocytes was observed by FITC-labeled RSV-PLGA-NPs with confocal microscopy.

2.4. Pharmacokinetics of RSV-PLGA-NPs in vivo

Thirty male SD rats (weighing 250 g) in this experiment were supplied by the Laboratory Animal Center of Zhengzhou University. All rats were maintained in a 12-h day: night cycle at 23 °C with unlimited water supply. After acclimation to the environmental conditions for 7 days, all rats are randomized into two groups, RSV and RSV-PLGA-NPs, respectively, the RSV group rats are treated with a single right knee joint injection of RSV suspension, the RSV-PLGA-NPs group is treated with a single right knee joint injection of RSV-loaded PLGA NPs, and 5 mg RSV or SV-PLGA-NPs dissolved in a 50 μL volume of dimethyl sulfoxide. Blood obtained from orbital vessels and knee tissue specimens were obtained to detect the concentrations of RSV in plasma and knee tissues, respectively, at the predetermined time after a single intra-articular injection. The RSV concentrations were detected by liquid chromatography–tandem mass spectrometry (LC-MS/MS) [13]. The pharmacokinetic parameters were calculated using the WinNonlin pharmacokinetic analysis program (Pharsight, v1.5, USA). Animal experiments were approved by experimental animal ethics committee of Luoyang Orthopedic Traumatology Hospital (Orthopedics Hospital of Henan Province) (Approval No.: KY2021-006-02).

2.5. Induction of OA and treatment

The rat osteoarthritis model was constructed by destabilizing the medial meniscus [14]. All rats (n = 40) were randomly divided into 3 groups as follows: sham surgery (control group), osteoarthritis model group (OA group), RSV-loaded PLGA NP treatment group (RSV group). Resveratrol (10 μM) dissolved in 0.02 % DMSO (10 μL) was administered once four weeks for 12 weeks in the right knee of RSV group after DMM surgery. The control and OA groups received 10 μL DMSO (0.02 %) in the right knee via intra-articular injection as similar to those described in RSV group. Following the last Magnetic Resonance Imaging (MRI) at week 12, all rats were sacrificed and their right knee tissues were collected for histological assessment.

2.6. MRI analysis

To assess the therapeutic effectiveness of RSV-loaded PLGA NPs, three rats were randomly chosen from each group for MRI using a 7 T MRI System (MAGNETOM Skyra, Siemens, Germany) 4, 8, 12 weeks after surgery. Anesthesia was performed with an isoflurane–oxygen mixture through inhalation. A 72-mm i. d. birdcage coil was applied as the transmitter coil, and a separate quadrature surface coil (Bruker, Ettlingen, Germany) was positioned at the knee joint tissues to reach maximum signal reception. All experiments were performed on an Oxford Instruments (Bruker) 200/300 magnet (33-cm clear bore, 4.7 T) equipped with a 16-cm i. d. actively-shielded Oxford gradient coil (200 μs rise time, 18 G/cm). The scanning sequence included SE T1WI (TR/TE = 205 ms/2.5 ms), SE T2WI (TR/TE = 3699 ms/45 ms), GRE T2 × WI (TR/TE/turn angle = 408 ms/3.5 ms/30°). The scanning direction was sagittal, the layer thickness was 1 mm, the matrix was 256 × 256, and the field of vision was 4 cm × 4 cm–5 cm × 5 cm. During the scanning, the rats were anesthetized with isoflurane gas, and the monitoring breath was maintained at about 60 times/min.

2.7. Histologic analysis

The entire knee joints were removed, and the surface of cartilage was photographed using a digital camera. Then, the joint tissues were fixed in paraformaldehyde (4 %) in PBS (0.1 M) overnight at 4 °C, decalcified with 10 % EDTA for 2 weeks, and embedded in paraffin wax. The sample

from each joint was paraffin-embedded, and cut into 5-mm sections for safranin O-fast green and hematoxylin and eosin (H&E) staining. The severity of osteoarthritis was determined in the medial compartment of the tissue sections (n = 5 per mouse) according to the Osteoarthritis Research Society International (OARSI) scoring system [15]. Cartilage thickness was evaluated by three blinded experts according to a previously described method [16].

2.8. TEM assay

Specimens from the cartilage from medial femoral condyles were fixed in glutaraldehyde (2 %) for 24 h. Then, the samples were cut into 1 mm^3 and postfixed with 1 % OsO4 and embedded in epoxy resin. Next, the tissues were sectioned into 80-nm thickness and stained with lead citrate and uranyl acetate. Lastly, the ultrathin slides were examined using a TEM (Phillips CM-80, Eindhoven, Netherlands).

2.9. Quantification of sGAG, CTXII, IL-1β, TNF-α

The urea standardization method was used to determine the dilution factor of synovial fluids lavages, and the concentration of each biomarker were adjusted based on the dilution factor [17]. SF lavage sGAG levels, a marker of proteoglycan turnover, were determined by Alcian Blue dye binding assay (Alpco Diagnostics, Windham, NH, USA) [18]. The content of GAGs in the sample was determined based on the chondroitin sulfate standard curve. The concentration of CTXII, a biomarker of collagen II breakdown, in the synovial fluid lavages was evaluated with serum preclinical Cartilaps ELISA kits (IDS, The Boldons, UK). Meanwhile, the concentrations of TNF-α and IL-1β were detected with commercially available ELISA kits (Invitrogen, CA, USA).

2.10. Real-time PCR

To further study the impact of resveratrol on the synthesis of extracellular matrix in articular cartilage, SYBR Green real-time PCR was conducted to measure the relative gene expression. Total RNA was extracted using the RNeasy kit (Qiagen). cDNA synthesis was conducted using the iScript Reverse Transcriptase kit (Bio-Rad). RNA quantification was then carried out on an ABI Prism 7700 system (Applied Biosystems) using the LightCycler-FastStart-DNA-Master-SYBR-green-I (Takara). The predesigned primer sequences for ADAMTS5, MMP13, COL2A1, aggrecan, and GAPDH were synthesized by Takara Bio (Table 1).

2.11. TUNEL assay

TUNEL assay was carried out with in situ apoptosis detection kit (KeyGEN Biotech, Nanjing, China). After digestion with 20 lg/ml proteinase K for 15 min, the serial sagittal sections of cartilage were immersed in 3 % H_2O_2 for 5 min and exposed to terminal deoxynucleotidyl transferase for 1 h at 37 °C. Next, the sections were exposed to antidigoxigenin-peroxidase antibody for 30 min at 37 °C, followed by visualization with diaminobenzidine and counterstaining with hematoxylin. The chondrocytes with brown nuclei were considered positive. The number of TUNEL-positive cells was detected under a fluorescence microscope.

2.12. Immunohistochemistry

The paraffin-embedded specimens were deparaffinized in xylene, followed by rehydration in graded ethanol and water. After rinsing with PBS, the sections were inhibited with 5 % serum for 30 min at RT, followed by incubation with rabbit anti-LC3 polyclonal antibody (1:50; Abgent, CA, USA), anti-P62 polyclonal antibody (1:100; Abgent), or anti-caspase 3 polyclonal antibody (1:200; Abgent) overnight at 4 °C. After rinsing with PBS, the sections were exposed to the secondary antibody Alexa Fluor 488 anti-rabbit IgG for 30 min. Lastly, the slides were rinsed and mounted with Prolong Gold Antifade Reagent (Invitrogen).

2.13. Statistical analysis

All values are shown as mean ± standard deviation (SD). All statistical tests were conducted using the SPSS 16.0 statistic software (SPSS Inc., IL, USA). Multiple pairwise comparisons were adjusted using Bonferroni correction. Kruskal-Wallis ANOVA was employed to determine differences in OARSI scores and the concentrations of sGAG, CTXII, TNF-α and IL-1β, in synovial fluid lavage across treatment groups. The MRI variables were examined by two-way ANOVA with repeated measures to examine intergroup variability over time and between treatment and control groups. Other data were analyzed with one-way ANOVA followed by Tukey's multiple comparison tests (*t*-test). *P*-values <0.05 (two-tailed) were deemed statistically significant.

3. Results

3.1. The properties of RSV-loaded PLGA NPs

The characteristics of RSV-loaded PLGA NPs were determined according to the comprehensive investigation results of preparation conditions. The final preparation conditions are as follows: the organic/aqueous phase (volume ratio) is 4:1, the ratio of RSV and PLGA in organic phase is 1: 9 (w/w), the concentrations of PLGA and PVA are 100 mg ml^{-1} and 3 %, respectively. The average particle size and polydispersity index of RSV-loaded PLGA NPs were 50.40 nm and 0.217, respectively (Fig. 1A). Moreover, the zeta potential of PLGA and RSV-loaded PLGA NPs were positively charged at 6.52 ± 0.11 and 12.57 ± 1.32, respectively. The SEM results showed that the microspheres were round, regular in shape and uniform in size, and there was no adhesion between the microspheres. The particle size is about 50 nm (Fig. 1G). Three batches of RSV-loaded PLGA NPs were prepared under the optimized conditions. HPLC analysis revealed that the average EE and DL of RSV-loaded PLGA NPs were 92.35 % and 15.1 %, respectively. The FTIR spectral characteristics of RSV, RSV-PLGA-NPTs, and PLGA-

Table 1
Primer pairs for RT-PCR.

Gene		Sequences (5′–3′)	Product size (bp)	Accession no.
COL2A1	Forward	AGGGCCAGGATGTCCGGCA GGGTCCCAGGTTCTCCATCT	195	NM_001844
Aggrecan	Forward	CAACTACCCGGCCATCC GATGGCTCTGTAATGGAACAC	160	NM_013227
MMP13	Forward	GGAGCATGGCGACTTCTAC GAGTGCTCCAGGGTCCTT	208	NM_133530.1
ADAMTS5	Forward	GCCAGCGGATGTGTGCAAGC ACACTTCCCCCGGACGCAGA	130	NM_198761.1
GAPDH	Forward	CCCTCAATGACCGTG GGTTTGAGGGCTCTTACTCCT	143	NM_017008.3

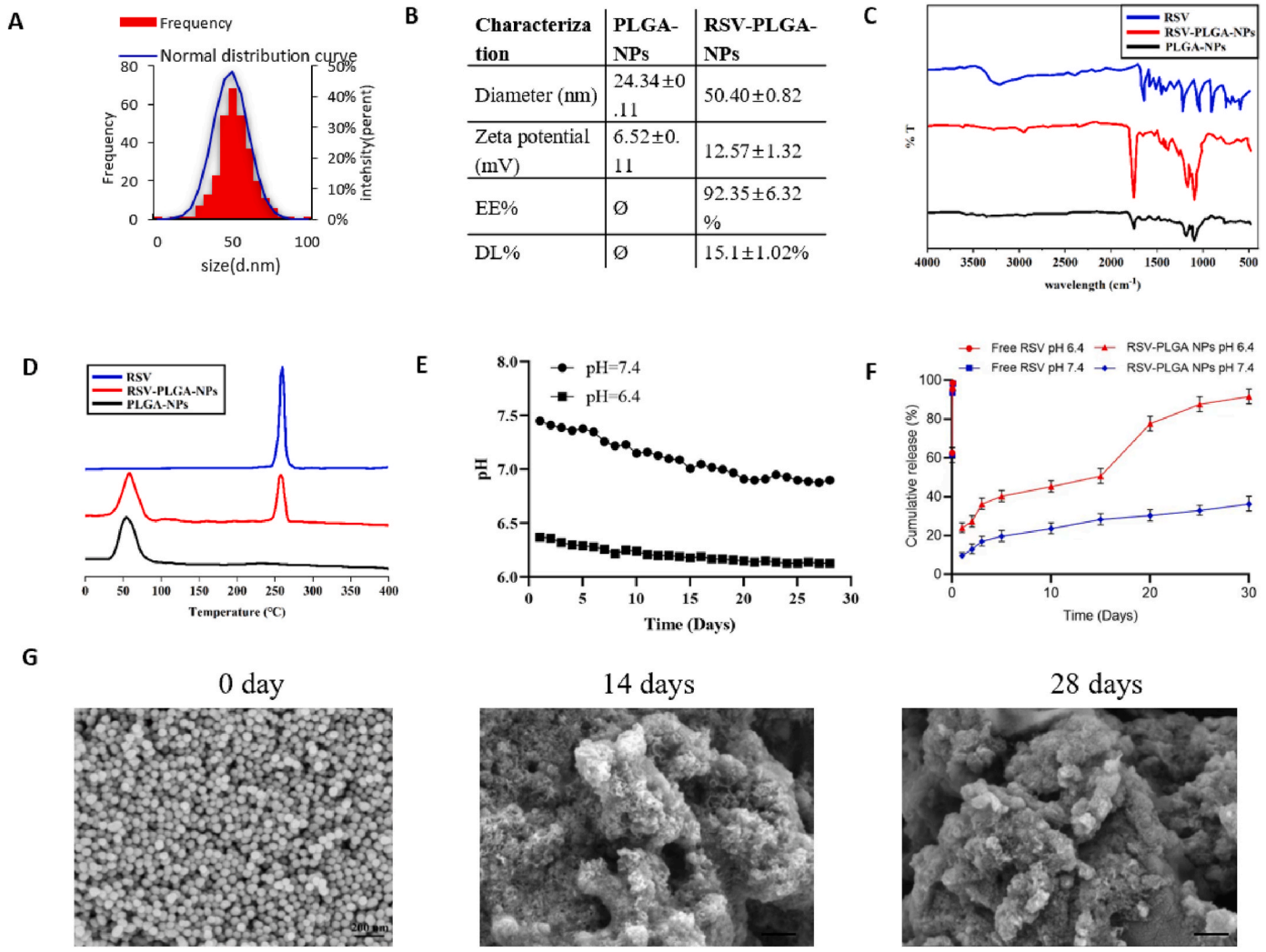

Characterization	PLGA-NPs	RSV-PLGA-NPs
Diameter (nm)	24.34±0.11	50.40±0.82
Zeta potential (mV)	6.52±0.11	12.57±1.32
EE%	Ø	92.35±6.32 %
DL%	Ø	15.1±1.02%

Fig. 1. The characterization of RSV-PLGA-NPs. (A) Frequency and particle size distribution, (B) characterization, (C) FTIR spectra for RSV-PLGA-NPs, (D) DSC, (E) Drug cumulative release profile, (F) Degradation in vitro and (G)SEM of degradation in vitro.

NPs were shown in Fig. 1C. RSV-PLGA-NPs had all the characteristic absorption peaks of PLGA-NPs and RSV. Differential scanning calorimetry (DSC) results showed that white RSV was completely wrapped in PLGA NPs (Fig. 1D).

The release profiles of RSV from RSV-loaded PLGA NPs are shown in Fig. 1F, Fig. S2. To investigate the drug release rate of RSV-loaded PLGA NPs in different pH environments, we examined the release profiles of RSV in PBS at Ph 7.4 and Ph 6.4, respectively. It was found that low pH significantly accelerated the release of RSV (There were two stages of drug release in vitro, the first 24 h was in the stage of sudden release, the cumulative release of RSV reached 31.64 %, and then entered the stage of slow release, the total cumulative release rate reached 52.14 % by the 10th day. From day 11, RSV-loaded PLGA NPs entered the second rapid release period. The cumulative release rate reached 95.45 % within 28 days.). It is clear that RSV-loaded PLGA NPs are capable of effective and sustained drug release under acidic OA conditions. To explore the release mechanisms, the release curves were drawn with different models. As shown in Fig. S3, the results showed that the release profile of RSV-loaded PLGA NPs conformed to the first-order kinetic model (R^2 = 0.9951) in vitro, which belonged to the diffusion-controlled release process.

In order to verify the in vitro degradation rate of RSV-PLGA-NPs and the change of pH value of RSV-PLGA-NPs in degradation under different pH conditions, we performed in vitro degradation experiments. As shown in Fig. 1E, acids are generated during degradation to lower the pH (Fig. 1E). The SEM results showed that the surface structure of the nanoparticles changed when simulating the culture medium for 14 days, indicating that the nanoparticles had been mostly degraded, and the degradation was basically complete at 28 days (Fig. 1G), which was consistent with the results of sustained release of drugs in vitro.

3.2. Evaluation of biologic activity and cellular internalization of RSV-PLGA-NPs

The chondro-protective effects of RSV-loaded PLGA NPs were explored. The human osteoarthritis chondrocytes stimulated by IL-1β were treated with various concentrations of RSV-loaded PLGA NPs (0, 1, 5, 10, 30, 60, 90, 120, 150 and 180 μM) for 48 h. As shown in Fig. 2A and B, the CCK-8 assay showed that RSV-loaded PLGA NPs could increase the viability of chondrocytes in a concentration-dependent fashion, when the dose was below 60 μM. In particular, 60 μg/mL of RSV-loaded PLGA NPs maximized cell growth compared to IL-1β control ($P < 0.001$). Therefore, the RSV-loaded PLGA NP concentration of 60 μg/mL was selected for further analyses.

The chondro-protective effects of RSV-loaded PLGA NPs were verified by FDA/PI live/dead assays. Notably, IL-1β resulted in a lower density of live cells (green) and a greater distribution of dead cells (red) in chondrocytes (Fig. 2C). This toxicity of IL-1β can be significantly

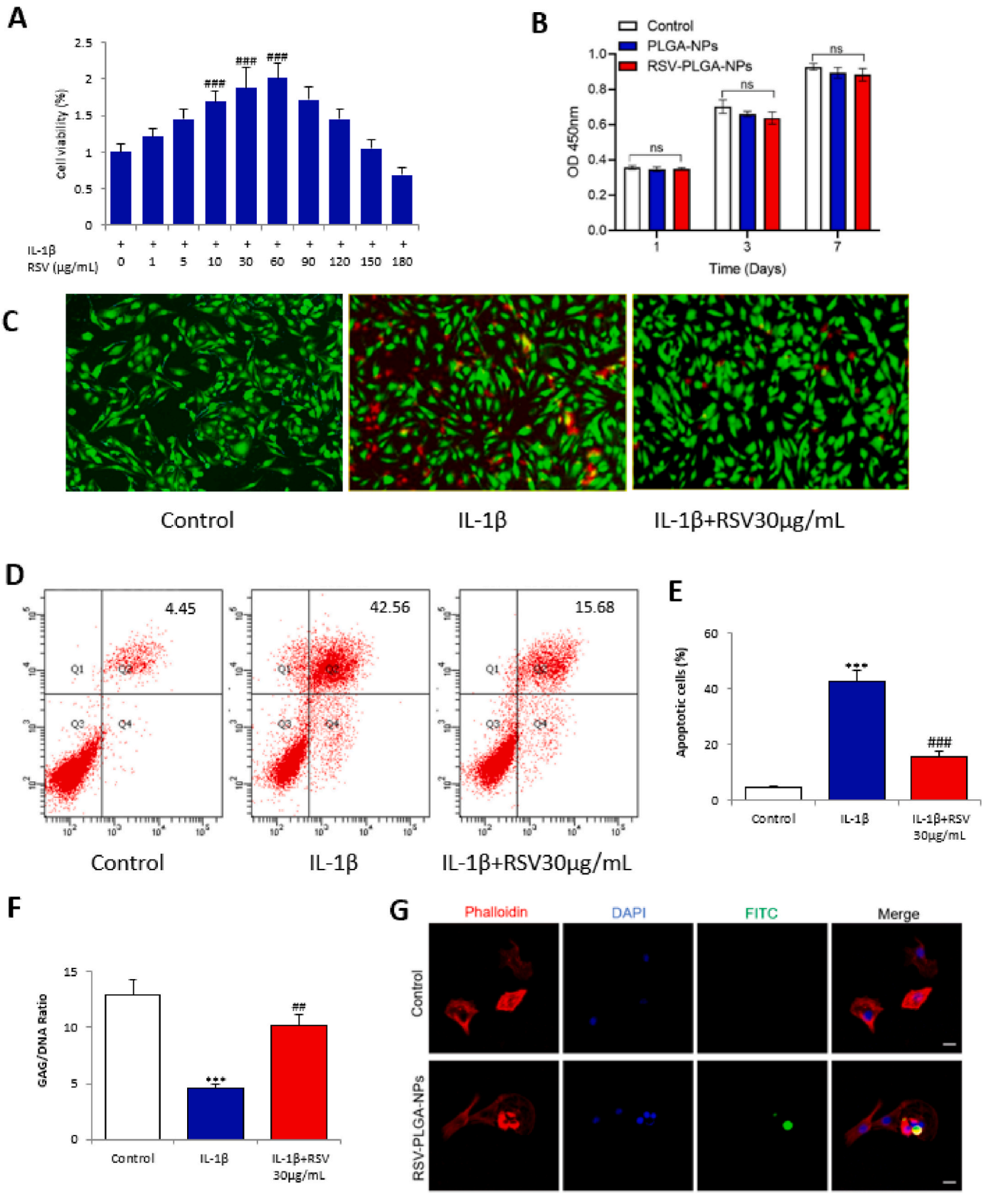

Fig. 2. Evaluation of biologic activity and cellular internalization of RSV-PLGA-NPs. (A–B) CCK assay was to detect the cytotoxicity of RSV-PLGA-NPs. (C) FDA//PI stained for cell viability, scale bar: 40 μm. (D) Flow cytometry for cell apoptosis. (E) Quantitative flow cytometry for apoptosis. (F) Quantification of matrix production of GAG (n = 6) for cell proliferation. (G) Image of chondrocytes internalizing RSV-PLGA-NPs, scale bar: 20 μm. Values are presented as means ± SD, n = 6. *Control versus IL-1β group, $^{\#}$ IL-1β versus RSV-PLGA-NPs group. $^{*\#}P < 0.05$, $^{**\#\#}P < 0.01$. $^{***\#\#\#}P < 0.001$.

inhibited by 60 μM RSV-loaded PLGA NPs. Flow cytometry was conducted to detect the cyto-protective effects of RSV-loaded PLGA NPs on chondrocyte apoptosis. As shown in Fig. 2D, E, a remarkable chondrocyte death with an increase level of apoptosis was observed in IL-1β-treated chondrocytes. On the contrary, RSV-loaded PLGA NP intervention obviously decreased IL-1β-stimulated chondrocyte apoptosis by 77.59 %.

GAGs are responsible for maintaining the integrity of the cartilage matrix. Deficiency of GAGs is an early change in osteoarthritis [19]. The 1,9-dimethylmethylene blue (DMMB) assay was performed to determine the effect of RSV-loaded PLGA NPs on GAG expression. As displayed in Fig. 2F, a remarkable loss of GAGs was observed in IL-1β-stimulated chondrocytes (up to 64.54 %). However, RSV-loaded PLGA NPs could rescue IL-1β-stimulated GAG loss by returning it to baseline levels.

In addition, in order to detect the uptake of nanoparticles in chondrocytes, we detected the intracellular fluorescence signal after 24 h of co-culture of FITC-labeled RSV-PLGA-NPs with chondrocytes, as shown in Fig. 2G, nanoparticles can be uptaken by chondrocytes.

3.3. Systemic exposure and joint retention of RSV after a single intra-articular administration of RSV-PLGA-NPs

The concentrations of RSV in both plasma and knee joint were determined by LC-MS/MS different time points after a single intra-articular administration of 5 mg of RSV-loaded PLGA NPs and RSV suspension. As shown in Fig. 3A, the plasma concentration of RSV was increased rapidly after administration of RSV suspension, reaching Cmax value of 6500.2 pg/mL after 4.1 h. This rapid drug efflux from the knee joint is consistent with the in vitro release performance, indicating that RSV suspension injected into articular cavity could be absorbed rapidly and passed through the gap junctions in synovial membranes. Upon reaching the peak concentration, the plasma concentration decreased rapidly below 300 pg/mL after 72-h administration of RSV suspension. On the contrary, the systemic exposure of RSV from RSV-loaded PLGA NPs was considerably lower than that of RSV suspension, and the duration of quantifiable levels of RSV was longer due to the extended release mechanism of the PLGA microsphere. The Cmax value of RSV in 12.4 h following intra-articular injection of RSV-loaded PLGA NPs was determined to be 1200.5 pg/mL. Then, it began to decline gradually, and reached below the limit of quantitation 35 days after injection with RSV-loaded PLGA NPs. As demonstrated in Fig. 3B, RSV-loaded PLGA NPs markedly decreased the redistribution of dissolved and/or micronized compounds into the bloodstream, thus prolonging the retention time of RSV in joint tissues.

In addition, the concentrations of RSV in the knee cartilage samples of osteoarthritis rats were assessed (Fig. 3C). After the intra-articular administration of RSV suspension, the concentration of RSV in the joint tissue was only 856 pg/mL at day 3, and below the lower limit of quantification at day 5. On the other hand, RSV-loaded PLGA NPs showed a significantly profound and prolonged concentration profile in joint tissues compared to RSV suspension, with measurable RSV concentrations over 35 days. The concentration of RSV in joint tissues reached 120 ng/g at day 3 after intra-articular injection of RSV-loaded PLGA NPs. These findings suggest that the retention time of RSV in joint tissues is prolonged due to the sustained-release property of RSV-loaded PLGA NPs.

3.4. Effect of RSV-PLGA-NPs on articular cartilage

Representative $T_{1\rho}$ and T_2 maps of the rats knee joints in control, OA and RSV-loaded PLGA NPs groups at 4, 8 and 12 weeks during administration are shown in Fig. 4A. Compared to control group, the $T_{1\rho}$ values of OA group were remarkably elevated at week 4 in the medial femoral condyle (MFC) ($P < 0.05$), lateral tibia (LT) and medial tibia (MT) ($P < 0.01$) and at week 8 in lateral femoral condyle (LFC) ($P < 0.05$), MFC, MT and LT (all $P < 0.01$). At week 12, the $T_{1\rho}$ values of OA group were dramatically higher in MFC, LFC, LT and MT (all $P < 0.01$). The $T_{1\rho}$ values of RSV-loaded PLGA NPs group were obviously reduced

A

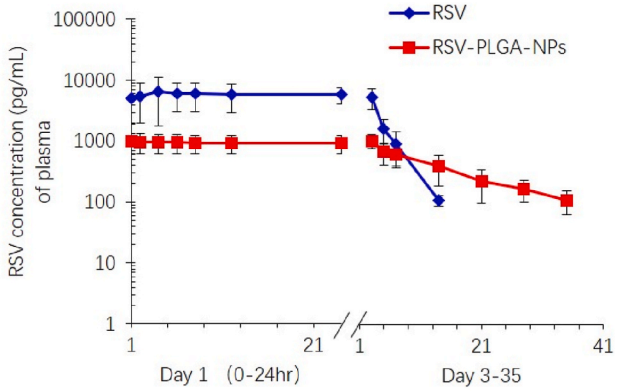

C

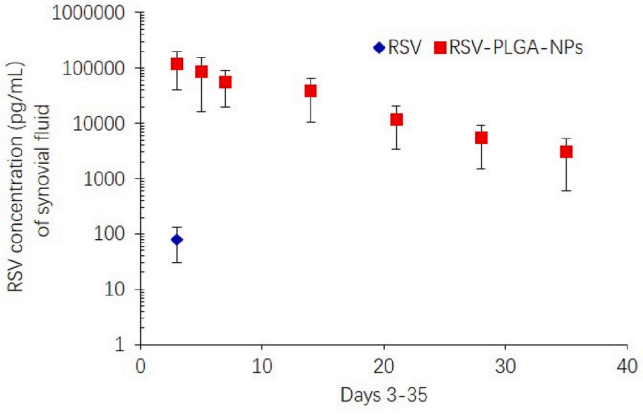

B

Parameters	RSV suspension	RSV-PLGA-NPs
C_{max} (pg/g)	6500.2	1200.5
T_{max} (h)	4.1	12.4
$T_{1/2}$ (h)	75.2	352.6
$AUC_{0\text{-}24h}$ (pg·h/mL)	113,625.4	11,108.2
$AUC_{0\text{-}35d}$ (pg·h/mL)	Not assessed	108,658.6
$AUC_{0\text{-}\infty}$ (pg·h/mL)	Not assessed	165,475.8

Fig. 3. RSV concentrations (log-linear scale) of blood plasma and synovial fluid over time following a single intra-articular injection of RSV-PLGA-NPs or RSV.

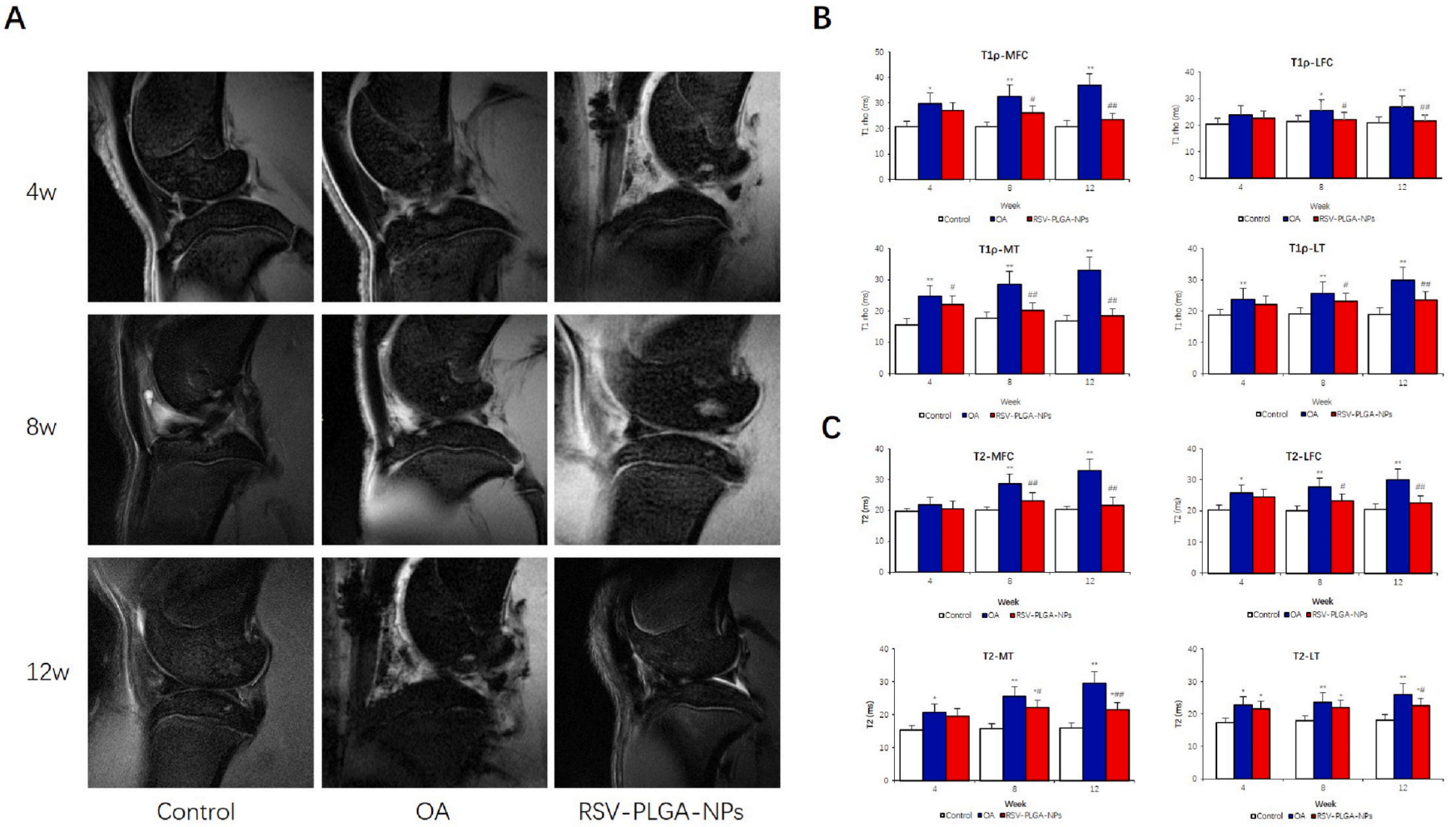

Fig. 4. Representative articular cartilage $T_{1\rho}$ and T_2 maps of Control, OA, RSV-PLGA-NPs treated knee joints 4, 8, 12 weeks after RSV-PLGA-NPs treatment. Maps are overlaid on Multi Gradient Echo images (A). The $T_{1\rho}$ values of RSV-PLGA-NPs group rats were obviously reduced compared to the OA group at 4 weeks in MT, at 8 weeks in MT, MFC, LFC, and LT and at 12 weeks in MFC, LFC, LT and MT (B). The T2 values of RSV-PLGA-NPs treated rats were significantly higher compared to control group in MT and LT at 8 and 12 weeks (C). Results are reported as mean ± SD (n = 5). *Control versus OA group, $^{\#}$OA versus RSV-PLGA-NPs group. $^{*\#}P < 0.05$, $^{****\#\#}P < 0.01$.

compared to those of OA group at week 4 in MT ($P < 0.05$), week 8 in MT ($P < 0.01$), MFC, LFC and LT (all $P < 0.05$) and week 12 in LFC, MFC, MT and LT (all $P < 0.01$) (Fig. 4B).

Similarly, the T_2 values of OA group were remarkably higher at week 4 in LT, MT and LFC (all $P < 0.05$), as well as weeks 8 and 12 in LFC, MFC, LT and MT (all $P < 0.01$) compared to control group. The T_2 values of RSV-loaded PLGA NPs group were markedly decreased compared to OA group at week 8 in MFC ($P < 0.01$), LFC and MT (all $P < 0.01$) and at week 12 in LT ($P < 0.05$), MFC, MT and LT (all $P < 0.01$). The T_2 values of RSV-loaded PLGA NPs group were dramatically higher than those of control group at week 8 and 12 in MT and LT ($P < 0.05$) (Fig. 4C).

3.5. Effect of RSV-PLGA-NPs on histomorphology of OA rats

First, gross morphology of the tibial plateau and femoral condyle was observed. As shown in Fig. 5A, the articular cartilage surface of sham-operation group was showed an integral, smooth surface with no defects and osteophyte formation, while articular cartilage destruction, as characterized by surface erosion, fibrillation, pitting, osteophyte formation, subchondral bone exposure and ulceration, was detected. However, injection of RSV nanoparticles significantly reduced cartilage damage, and its sliding cartilage surface was similar to that of normal cartilage.

Histopathological analyses by Safranin O-fast green and H&E staining indicated that normal articular cartilage overlying the cancellous bone and subchondral bone plate was observed, of which the superficial layers were smooth with integrity. In addition, the chondrocytes were arranged in flat and orderly rows, and the cartilage matrix was stained with saffron in control group. The OA group demonstrated severe pathologic changes, such as clustered chondrocytes, fibrillation and fissures, osteophyte proliferation, defects in cartilage superficial zone, subchondral trabecular bone loss with the bone marrow spaces occupied by synovitis, subchondral bone cyst and fibrous tissue. Compared with OA group, RSV group had disorganization and loss of chondrocytes, a significant improvement in fissures, an increase in safranin-O unstained area and reduced synovitis (Fig. 5B and C). MRI scanning showed the number and area of osteophytes increased significantly around the joints in OA group (Fig. 5D). In contrast, in the RSV-PLGA-NPs group, the number and surface area of osteophytes were less than those in the OA group.

The OARSI score was employed to analyze cartilage destruction, osteophyte formation, subchondral bone and synovitis. The median OARSI scores in the medial tibial plateau and femoral condyle were markedly reduced in RSV group compared with OA group (Fig. 5E). In addition, RSV nanoparticles significantly attenuated osteophyte formation, subchondral plate thickness and synovitis (Fig. 5F,G,H).

3.6. TEM analysis of chondrocyte morphology

TEM imaging showed that the normal chondrocytes were round or spindle shaped with short microvilli like protrusions extending to the cartilage lacuna on the cell surface; the nucleus was slightly round; the chromatin was evenly distributed; the cytoplasm was still within free ribosomes; the golgi apparatus and microfilaments were observed (Fig. 6A, B, C). However, the chondrocytes in OA group had poor structure, irregular shape of nucleus, agglutination of chromatin in nucleus, more lipid droplets and focal dissolving areas in cytoplasm, and reduced number of other organelles (Fig. 6D, E, F). However, following administration of 1000 μg/mL RSV-loaded PLGA NPs, chondrocyte nuclei showed more integrity, and the mitochondria were arranged in rows with relatively complete structure (Fig. 6G, H, I). The formation of autophagic lysosomes was indicated by the arrow.

3.7. Effects of RSV-PLGA-NPs on expression of catabolic mediators in cartilage and levels of GAGs, CTX-II, IL-1β, and TNF-α in the synovial fluid lavages from OA rats

Expression of the catabolic markers MMP13 and ADAMTS-5 in cartilage tissue was inhibited by intra-articular administration of RSV-loaded PLGA NPs, and the reduced expression of AGG and Col-II in articular cartilage was rescued by RSV-loaded PLGA NPs (Fig. 7A).

At baseline, the synovial lavage concentrations of GAGs, CTX-II, IL-1β and TNF-α were no significantly different between the control, OA and RSV treatment groups. The synovial lavage levels of GAGs, CTX-II, TNF-α and IL-1β were markedly upregulated in OA group compared with control group at 12 postoperative weeks. In RSV treatment group, GAGs, CTX-II, TNF-α and IL-1β levels were markedly reduced compared with OA group at week 12 (Fig. 7B).

3.8. Effects of RSV-PLGA-NPs on chondrocyte apoptosis and autophagy of OA rats

TUNEL staining results showed that chondrocyte apoptosis was induced in the joint tissues of osteoarthritis rats, but blocked by RSV-loaded PLGA NPs treatment (Fig. 8A). Furthermore, immunohistochemical analysis indicated that the chondrocytes in OA group had higher levels of caspase-3 than control group, implying that osteoarthritis could induce chondrocyte apoptosis. RSV-loaded PLGA NPs remarkably inhibited overexpression of cleaved caspase-3 (Fig. 8B). It was also observed that RSV-loaded PLGA NPs significantly activated autophagy, as revealed by the formation of LC3 and degradation of p62 (Fig. 8C), which is consistent with our previous findings [7]. The above results indicated that intra-articular RSV-loaded PLGA NPs could inhibit the matrix degrading enzyme activities and chondrocyte apoptosis to delay osteoarthritis progression.

4. Discussion

In the current study, the effects of intra-articular administration of RSV-loaded PLGA NPs on osteoarthritis rats were investigated. PLGA has been extensively applied as a drug carrier, owing to its low biodegradability, biocompatible and systemic toxicity [20]. We first successfully synthesized RSV-loaded PLGA NPs and detected the properties and biological activity in vitro. The in vitro results showed that RSV-loaded PLGA NPs had spherical morphology with a negative charge of 12.57 ± 1.32 mV and a mean size of 50.40 nm. These nanoparticles had significant EE (92.35 %) and DL (15.1 %) for RSV. The controlled release of resveratrol pattern conformed to the first-order kinetic model. The synthesized RSV-loaded PLGA NPs demonstrated significant chondro-protective and anti-apoptotic effects on IL-1β stimulation in vitro. Besides, *in vivo,* we found that RSV-loaded PLGA NPs could retain in the synovium over a longer period of time, indicating a prolonged controlled release of RSV from RSV-loaded PLGA NPs. The imaging and histological results of this study confirmed that intra-articular injection of RSV-loaded PLGA NPs delayed articular cartilage destruction and subchondral trabecular bone changes in osteoarthritis rat model with destabilization of the medial meniscus (DMM). Thus, RSV-loaded PLGA NPs can serve as a potential intra-articular drug delivery system for preventing joint deterioration during osteoarthritis.

Considering that the joint has low bioavailability for systemic administration and rapidly eliminates drugs following intra-articular administration, it still remains a challenge for drug delivery. Nanoparticles can overcome the challenges of intra-articular drug delivery, as they improve biodistribution and drug residence time in the joint, and have the capacity to penetrate extracellular matrix and cell barriers, thus affecting the localization of drugs within specific joint tissues [21]. Although several physical parameters have been proposed for cartilage matrix structure and pore size, controversial results have been published regarding the threshold size of nanoparticles, which can prohibit matrix

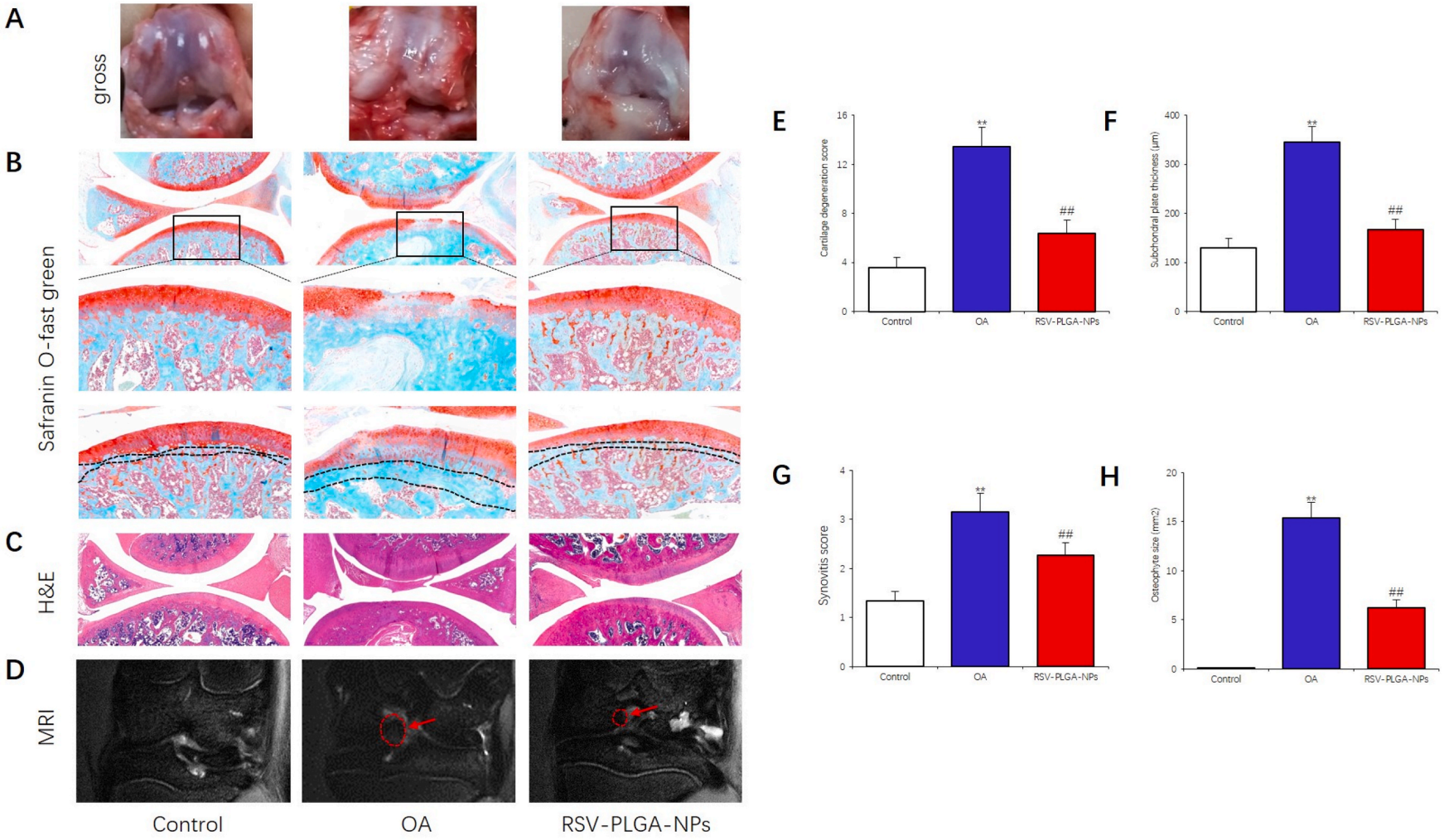

Fig. 5. RSV-PLGA-NPs intra-articular injection attenuate cartilage degeneration in OA model rats assessed by histological evaluations. (A) Gross images of the femoral condyle. (B) Safranin-O/Fast green staining of the joints. 50 × magnification (C) Hematoxylin and eosin staining of the synovium. 50 × magnification. (D) MRI scans of knee joint; there were bigger osteophyte formation around the joints in the OA group. (E) OARSI scores of articular cartilage. (F) subchondral plate thickness. (G) synovitis scores. (H) osteophyte size. All data represent mean ± SD (n = 5). *Control versus OA group, $^{\#}$OA versus RSV-PLGA-NPs group. $^{*\#}P < 0.05$, $^{**\#\#}P < 0.01$.

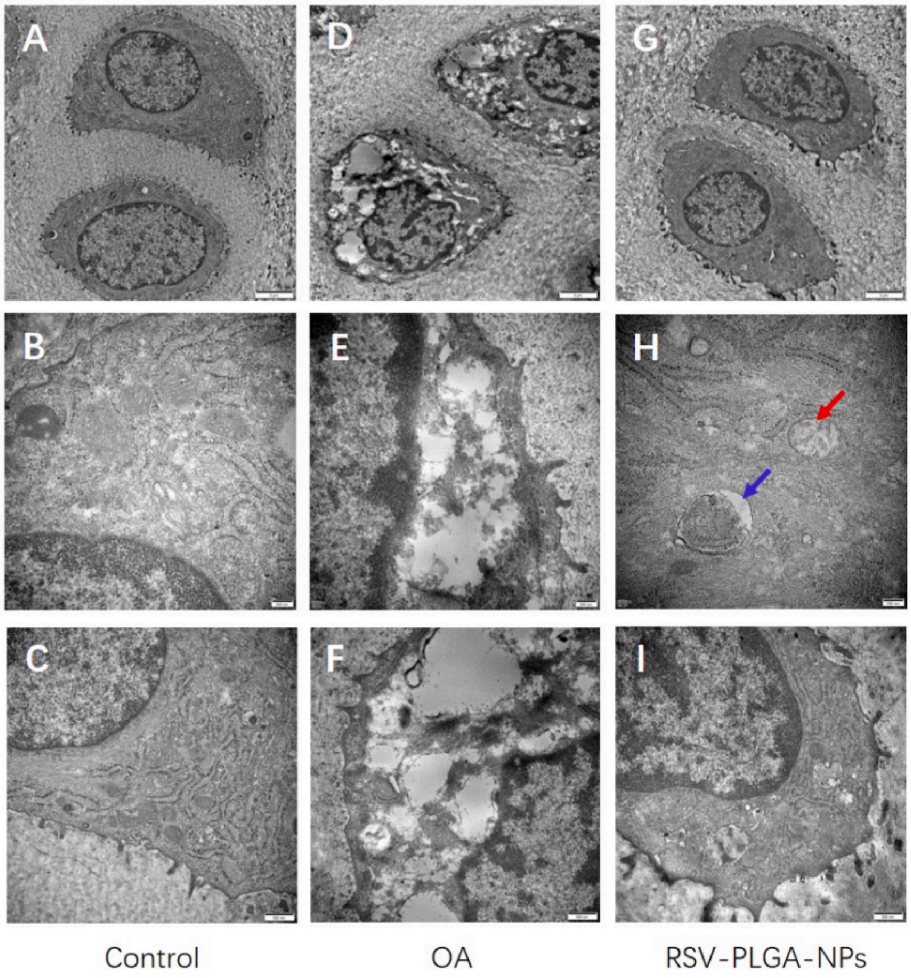

Fig. 6. Effect of RSV-PLGA-NPs on ultrastructural morphology of chondrocytes. (A, B, C) Control group, (D, E, F) OA group, (G, H, I) RSV-PLGA-NPs treated group. The ultrastructural morphology of chondrocytes was observed using TEM. Scale bar: 2 μm (A, D, G), bar: 200 μm (B, E, H), bar: 500 μm (C, F, I). autophagosome (red arrows), autophagic lysosome (blue arrows).

penetration. Previous research has suggested that nanoparticles (~55 nm) can penetrate through the full-thickness cartilage [22]. An abundance of extracellular matrix in avascular cartilage may hinder drug penetration, and the NPs (30–50 nm) can be taken up by cells and retained in the joint [23]. In our study, RSV-loaded PLGA NPs with a mean size of 50.40 nm had excellent properties within this optimal nanoparticle size range. Apart from particle size, the particle charge is a factor that affects the penetration and retention of cartilage matrix [24]. Another passive targeting strategy for cartilage is the intentional control over nanoparticles' zeta potential. The dense network of sulfated proteoglycans provides a bulk anionic charge to the cartilage [25,26], which corresponds to a proteoglycan level or fixed charge density of −158 to −182 mM in human articular cartilage [27]. Positively charged drug carriers demonstrated higher uptake and faster penetration than their neutral same-sized counterparts [28]. The RSV-loaded PLGA NPs synthesized in this study displayed positive zeta potential values, which could promote their prolonged interaction with the cells and mucus membranes [29,30], and therefore allowing the drug to penetrate well into the articular cartilage. Besides, tunable surface charge is also an important feature for successful intra-articular drug delivery. It has been found that positively charged nanocarriers can effectively bind and penetrate cartilage through reversible electrostatic interactions with anionic cartilage matrix proteoglycans [31].

Acidosis is a typical characteristic of arthritic joints, owing to insufficient vascular supply and increased metabolic activity [32]. Acidic extracellular pH can increase the responsiveness of nanoparticles in the inflamed synovium. Accordingly, RSV-loaded PLGA NPs were placed into PBS solution at pH 7.4 and 6.4 to stimulate normal and osteoarthritis synovial fluids, respectively. The results suggest that the prolonged release phase of RSV-loaded PLGA NPs is maintained for a period of time reaching 28 days after a short initial burst release of 26.92 % of total DL in the first three days, due to the lower release under acidic condition than neutral condition. *In vitro* release experiments have shown that RSV-loaded PLGA NPs were capable of achieving long-term release. This is due to the fact that the use of PLGA nanoparticles to encapsulate resveratrol can form stable nanocomplexes, effectively preventing degradation and inactivation of the drug and prolonging the half-life of the drug. Besides, some studies have also shown that RSV-loaded PLGA NPs can remain biologically active during prolonged release in vitro [12,33]. The *in vivo* pharmacokinetic study indicated that the concentration of RSV in synovial tissues following intra-articular administration of RSV-loaded PLGA NPs achieved its maximum concentration of 311.6 ng/g on the first day, and slowly decreased to 10 ng/g at day 28. Although intra-articular administration of resveratrol can slow down degradation and increase bioactivity when compared to systemic administration [34], we could not ensure that some degradation of resveratrol did not occur during the prolonged extended release over 30 days, and this remains to be addressed in our future studies. In a word, these *in vivo* and in vitro results demonstrated that RSV-loaded PLGA NPs can be applied for long-lasting and controlled-release intra-articular drug delivery.

To assess the biological effectiveness of RSV-loaded PLGA NPs, the

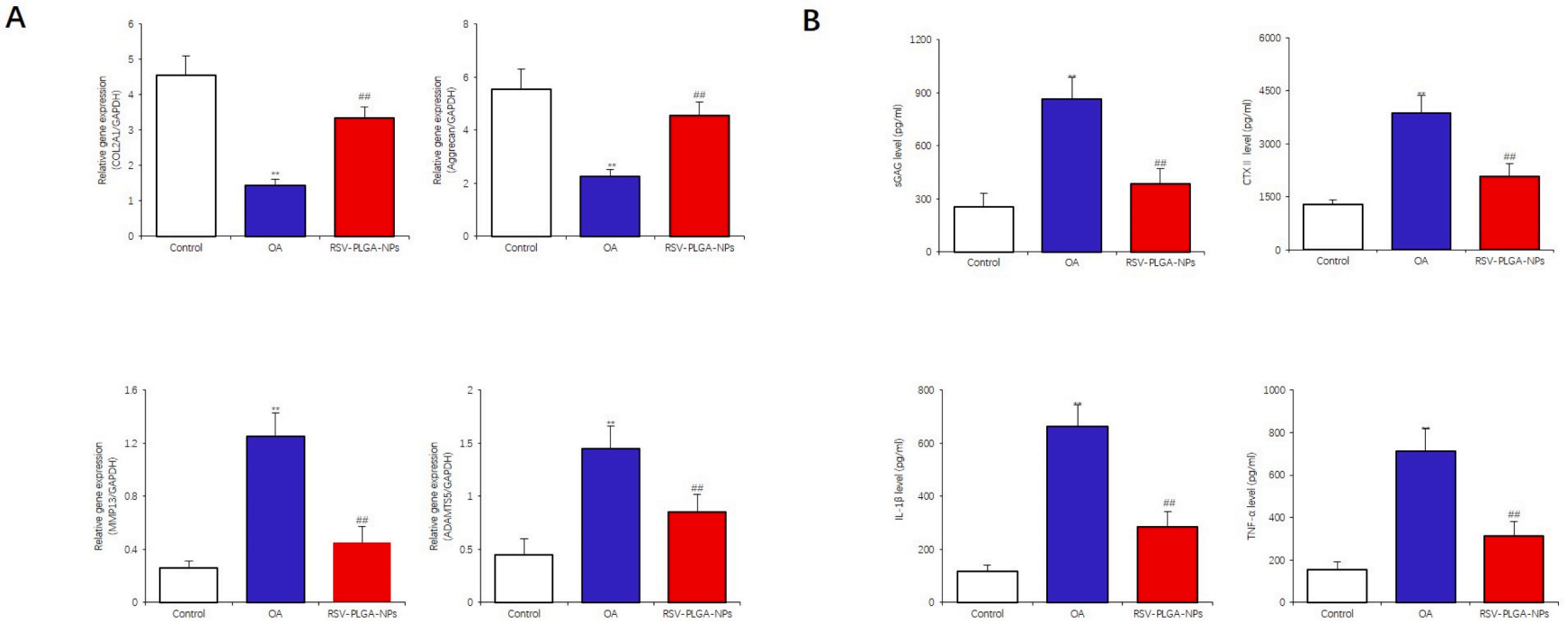

Fig. 7. Effects of RSV-PLGA-NPs on expression of catabolic mediators in cartilage and levels of GAGs, CTX-II, IL-1β, and TNF-α in the synovial fluid lavages from all groups. (A) QRT-PCR was used to analyze the mRNA expression levels of MMP13 and ADAMTS-5, AGG and Col-II in cartilage. (B) ELISA was used to detect the levels of GAGs, CTX-II, IL-1β, and TNF-α in the synovial fluid lavages. Values are presented as means ± SD, n = 5. *Control versus OA group, $^{\#}$OA versus RSV-PLGA-NPs group. $^{*\#}P < 0.05$, $^{**\#\#}P < 0.01$.

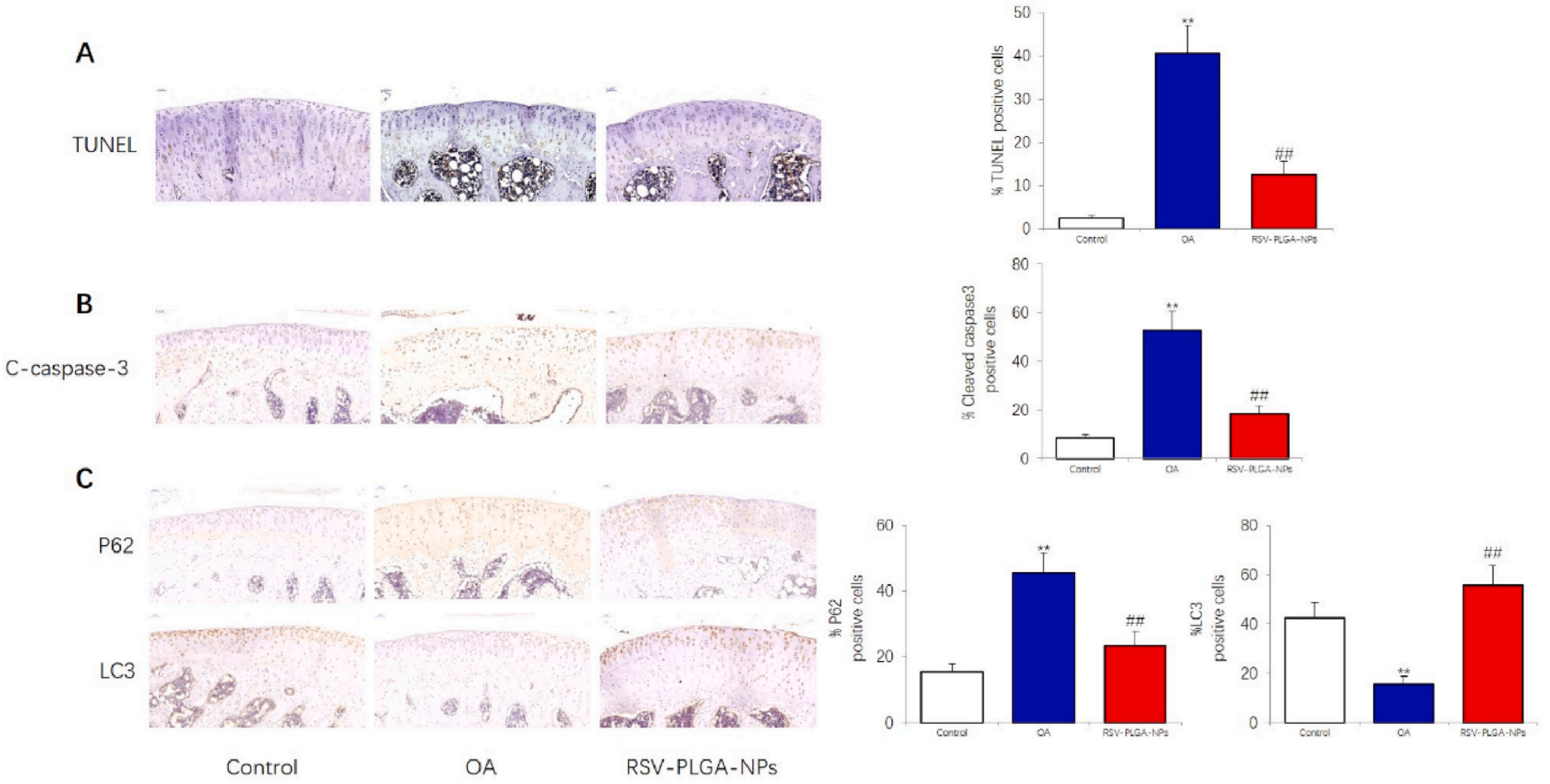

Fig. 8. Effects of RSV-PLGA-NPs on chondrocyte apoptosis and autophagy of OA rats. (A) TUNEL staining, 200 × magnification. (B) Immunohistochemical staining for Cleaved-caspase-3 (original magnification, × 200) and percentage of positive cells. (C) Immunohistochemical staining for P62, LC3 (original magnification, × 200) and percentage of positive cells. Representative immunohistochemical images are shown. Values are presented as means ± SD, n = 5. *Control versus OA group, $^{\#}$OA versus RSV-PLGA-NPs group. $^{**\#\#}P < 0.01$.

effects of free and encapsulated drugs on human articular chondrocytes were determined with IL-1β viability, apoptosis, inflammatory factor expression, extracellular matrix degradation and cellular internalization in vitro. A cascade of apoptosis and inflammatory events can be induced in arthritic chondrocytes, including the expression of MMPs, release of GAGs, and degradation of cartilage matrix [35]. The results of live/dead cell staining and MTT showed that RSV-loaded PLGA NPs significantly enhanced the cell viability and growth compared to the pure drug within the three-time intervals. Moreover, chondrocytes can function by internalizing RSV-loaded PLGA NPs into cells. RSV-loaded PLGA NPs obviously decreased the rate of IL-1β-stimulated chondrocyte apoptosis. Furthermore, our data indicated that RSV-loaded PLGA NPs significantly reduced the IL-1β-induced expression of inflammatory mediators (e.g., TNF-α and IL-6), and matrix-degrading enzymes (e.g., ADAMTS5 and MMP-13), suggesting that RSV-loaded PLGA NPs exert a protective role in the chondrocytes induced by IL-1β.

Then, the effectiveness of intra-articular administration of RSV-loaded PLGA NPs on DMM-induced osteoarthritis rat model was examined. MRI, with its recent advancements, has been extensively used to detect the changes in synovial membrane, subchondral bone marrow and cartilage [36–41]. The primary outcome measure used in this study was MRI, due to its superior contrast resolution and sensitivity to tissue compositions, as well as it ability to assess cartilage changes in osteoarthritis animal models [42,43]. T1ρ and T2 are important markers for determining the changes in cartilage during early phases of this disease [44,45]. Increased levels of T1r and T2 are related to hydration changes, collagen loss and proteoglycan loss in the cartilages [46].

Subsequently, histological analyses were conducted to determine the therapeutic effects of RSV-loaded PLGA NPs on osteoarthritis rats. Pathological changes in DMM-induced osteoarthritis, such as subchondral bone thickening, synovitis and cartilage destruction, were detected in human osteoarthritis [14]. Additionally, the OARSI scores were employed to detect the histomorphology of cartilages to reveal its biomechanical properties [47]. In the present study, the OARSI score analysis indicated the administration of RSV-loaded PLGA NPs markedly enhanced osteoarthritis-related pathological changes in the subchondral bone, synovium and cartilage degeneration, suggesting that RSV is a promising treatment for osteoarthritis.

Synovial tissue inflammation has been recognized as a pathogenic factor of the knee osteoarthritis. The levels of IL-1β and TNF-α in the synovial fluids have been reported to increase in osteoarthritis. Both IL-b and TNF-a exhibit catabolic action and perpetuate cartilage matrix degradation in osteoarthritis, including the suppression of type II collagen and activation of proteinase [48,49]. In our study, the cartilage breakdown products (e.g., sGAG and CTX-II) inflammatory markers (e.g., TNF-α and IL-1β) were elevated in osteoarthritis rats compared with sham-operated rats, which are in agreement with previous findings. Topical administration of RSV-loaded PLGA NPs effectively suppressed synovial tissue inflammation, cartilage and bone turnover rate in the osteoarthritis rat model. As expected, the expression levles of MMPs and ADAMTS genes were downregulated in IL-1β-stimulated chondrocytes after treatment with RSV-loaded PLGA NPs. These results corroborate the biochemical data obtained from *in vivo* study whereby RSV-loaded PLGA NPs remarkably attenuated the release of CTX-II and GAGs in DMM-induced osteoarthritis rats.

The progression of OA is often accompanied by the weakening of autophagic activity and resulting increase in the level of apoptosis [50,51]. Chondrocytes are the sole cellular constituents of normal cartilage. It has been reported that chondrocyte apoptosis is involved in the destruction of cartilage during osteoarthritis. Moreover, an increase in chondrocyte apoptosis has been anatomically linked to proteoglycan depletion [52]. Previous studies have suggested that RVS protects chondrocytes against apoptosis via different mechanisms, such as scavenging ROS [53], inhibiting mitochondrial membrane depolarization and ATP depletion [54], regulating the MALAT1/miR-9/NF-κB signaling pathway [55]. In the current study, tunel staining revealed that a massive amount of apoptotic chondrocytes was found upon DMM intervention compared to sham group, while the number of apoptotic chondrocytes was reduced in resveratrol-treated rats. In addition, the chondrocytes in OA group displayed a higher level of the apoptotic marker caspase-3 compared with sham operation rats, and this tendency was prominently attenuated by the intra-articular injection of RSV-loaded PLGA NPs. This implies that RSV-loaded PLGA NPs can effectively inhibit chondrocyte apoptosis, which is in agreement with our in vitro data. Taken together, our findings demonstrate that RSV-loaded PLGA NPs inhibit DMM-induced chondrocyte apoptosis, resulting in the efficient protection of articular cartilage.

In summary, RSV-loaded PLGA NPs were successfully prepared in our study, which demonstrated prominent effects of inhibition of chondrocyte apoptosis and promotion of GAG synthesis in vitro. Notably, the superiority of RSV-loaded PLGA NPs was supported by displaying a 35-day sustained release of RSV following a single intra-articular injection. Through intra-articular delivery in rats osteoarthritis model, RSV-loaded PLGA NPs reduced cartilage degradation, synovium, cartilage and bone turnover, and subchondral trabecular bone changes by suppressing cartilage matrix degradation, joint inflammation, chondrocyte apoptosis and promoting autophagy. Our findings suggest that intra-articular delivery of RSV via PLGA NPs might be an effective therapeutic approach for treating and preventing of osteoarthritis.

Funding statement

This work was supported by Health Commission of Henan Provincial, China (HNSWJW-2021016).

CRediT authorship contribution statement

Liwei Wei: Writing - original draft, Conceptualization, Formal analysis, Methodology. **Qingqing Pan:** Data curation, Writing - review & editing, Methodology. **Junyan Teng:** Investigation, Methodology, Validation, Writing - review & editing. **Hong Zhang:** Supervision, Project administration. **Na Qin:** Conceptualization, Funding acquisition, Supervision, Resources.

Declaration of competing interest

The authors have declared that no conflict of interest exists.

Data availability

Data will be made available on request.

Acknowledgements

The authors would like to express their gratitude to EditSprings (https://www.editsprings.com/) for the expert linguistic services provided.

Appendix A. Supplementary data

Supplementary data to this article can be found online at https://doi.org/10.1016/j.mtbio.2023.100884.

References

[1] D.J. Hunter, S. Bierma-Zeinstra, Osteoarthritis. Lancet. 393 (2019) 1745–1759.
[2] M. Varela-Eirin, J. Loureiro, E. Fonseca, S. Corrochano, J.R. Caeiro, M. Collado, et al., Cartilage regeneration and ageing: targeting cellular plasticity in osteoarthritis, Ageing Res. Rev. 42 (2018) 56–71.
[3] P.G. Conaghan, D.J. Hunter, J.F. Maillefert, W.M. Reichmann, E. Losina, Summary and recommendations of the OARSI FDA osteoarthritis assessment of structural change working group, Osteoarthritis Cartilage 19 (2011) 606–610.

[4] S. Yang, M. Sun, X. Zhang, Protective effect of resveratrol on knee osteoarthritis and its molecular mechanisms: a recent review in preclinical and clinical trials, Front. Pharmacol. 13 (2022), 921003.
[5] N. Pannu, A. Bhatnagar, Resveratrol: from enhanced biosynthesis and bioavailability to multitargeting chronic diseases, Biomed. Pharmacother. 109 (2019) 2237–2251.
[6] A.Y. Berman, R.A. Motechin, M.Y. Wiesenfeld, M.K. Holz, The therapeutic potential of resveratrol: a review of clinical trials, npj Precis. Oncol. 1 (2017) 35.
[7] N. Qin, L. Wei, W. Li, W. Yang, L. Cai, Z. Qian, et al., Local intra-articular injection of resveratrol delays cartilage degeneration in C57BL/6 mice by inducing autophagy via AMPK/mTOR pathway, J. Pharmacol. Sci. 134 (2017) 166–174.
[8] W. Li, L. Cai, Y. Zhang, L. Cui, G. Shen, Intra-articular resveratrol injection prevents osteoarthritis progression in a mouse model by activating SIRT1 and thereby silencing HIF-2a, J. Orthop. Res. 33 (2015) 1061–1070.
[9] L. Chen, Y. Wang, L. Sun, J. Yan, H.Q. Mao, Nanomedicine strategies for anti-inflammatory treatment of noninfectious arthritis, Adv. Healthcare Mater. 10 (2021), e2001732.
[10] D. Ding, Q. Zhu, Recent advances of PLGA micro/nanoparticles for the delivery of biomacromolecular therapeutics, Mater. Sci. Eng., C 92 (2018) 1041–1060.
[11] Y. Liu, X. Wu, Y. Mi, B. Zhang, S. Gu, G. Liu, et al., PLGA nanoparticles for the oral delivery of nuciferine: preparation, physicochemical characterization and in vitro/in vivo studies, Drug Deliv. 4 (2017) 443–451.
[12] S. Wan, L. Zhang, Y. Quan, K. Wei, Resveratrol-loaded PLGA nanoparticles: enhanced stability, solubility and bioactivity of resveratrol for non-alcoholic fatty liver disease therapy, R. Soc. Open Sci. 5 (2018), 181457.
[13] Y. Hsieh, HPLC-MS/MS in drug metabolism and pharmacokinetic screening, Expet Opin. Drug Metabol. Toxicol. 4 (1) (2008) 93–101.
[14] S.S. Glasson, T.J. Blanchet, E.A. Morris, The surgical destabilization of the medial meniscus (DMM) model of osteoarthritis in the 129/SvEv mouse, Osteoarthritis Cartilage 15 (2007) 1061–1069.
[15] S.S. Glasson, M.G. Chambers, W.B. Van Den Berg, C.B. Little, The OARSI histopathology initiative - recommendations for histological assessments of osteoarthritis in the mouse, Osteoarthritis Cartilage 18 (Suppl 3) (2010) S17–S23.
[16] W.J. Pinamont, N.K. Yoshioka, G.M. Young, V. Karuppagounder, E.L. Carlson, A. Ahmad, et al., Standardized histomorphometric evaluation of osteoarthritis in a surgical mouse model, J. Vis. Exp. 159 (2020), https://doi.org/10.3791/60991.
[17] V.B. Kraus, J.L. Huebner, C. Fink, J.B. King, S. Brown, T.P. Vail, et al., Urea as a passive transport marker for arthritis biomarker studies, Arthritis Rheum. 46 (2002) 420–427.
[18] S. Björnsson, Simultaneous preparation and quantitation of proteoglycans by precipitation with alcian blue, Anal. Biochem. 210 (1993) 282–291.
[19] M.E. Adams, M.E. Billingham, H. Muir, The glycosaminoglycans in menisci in experimental and natural osteoarthritis, Arthritis Rheum. 26 (1983) 69–76.
[20] B. Boltnarova, J. Kubackova, J. Skoda, A. Stefela, M. Smekalova, P. Svacinova, et al., PLGA based nanospheres as a potent macrophage-specific drug delivery system, Nanomaterials 11 (2021) 749.
[21] W. Zhang, R. Taheri-Ledari, F. Ganjali, S.S. Mirmohammadi, F.S. Qazi, M. Saeidirad, et al., Effects of morphology and size of nanoscale drug carriers on cellular uptake and internalization process: a review, RSC Adv. 13 (2022) 80–114.
[22] H.P. Erickson, Size and shape of protein molecules at the nanometer leveldetermined by sedimentation, gel filtration, and electron microscopy, Biol. Proced. Online 11 (2009) 32–51.
[23] L. Shang, K. Nienhaus, G.U. Nienhaus, Engineered nanoparticles interacting with cells: size matters, J. Nanobiotechnol. 12 (2014 Feb 3) 5.
[24] A.G. Bajpayee, A.J. Grodzinsky, Cartilage-targeting drug delivery: can electrostatic interactions help? Nat. Rev. Rheumatol. 13 (2017) 183–193.
[25] A.W. Palmer, R.E. Guldberg, M.E. Levenston, Analysis of cartilage matrix fixed charge density and three-dimensional morphology via contrast-enhanced microcomputed tomography, Proc. Natl. Acad. Sci. U. S. A. 103 (2006) 19255–19260.
[26] R. Stanescu, S.J. Leibovich, The negative charge of articular cartilage surfaces, Arthritis Rheum. 29 (1986) 573.
[27] E.M. Shapiro, A. Borthakur, A. Gougoutas, R. Reddy, 23Na MRI accurately measures fixed charge density in articular cartilage, Magn. Reson. Med. 47 (2002) 284–291.
[28] A.G. Bajpayee, C.R. Wong, M.G. Bawendi, E.H. Frank, A.J. Grodzinsky, Avidin as a model for charge driven transport into cartilage and drug delivery for treating early stage post-traumatic osteoarthritis, Biomaterials 35 (2014) 538–549.
[29] A. Di Martino, V. Sedlarik, Amphiphilic chitosan-grafted-functionalized polylactic acid based nanoparticles as a delivery system for doxorubicin and temozolomide cotherapy, Int. J. Pharm. 474 (2014) 134–145.
[30] W.H. Abd-Elsalam, N.A. ElKasabgy, Mucoadhesive olaminosomes: a novel prolonged release nanocarrier of agomelatine for the treatment of ocular hypertension, Int. J. Pharm. 560 (2019) 235–245.
[31] B.C. Geiger, S. Wang, R.F. Padera, A.J. Grodzinsky, P.T. Hammond, Cartilage-penetrating nanocarriers improve delivery and efficacy of growth factor treatment of osteoarthritis, Sci. Transl. Med. 10 (2018), eaat8800.
[32] J.R. Levick, Hypoxia and acidosis in chronic inflammatory arthritis; relation to vascular supply and dynamic effusion pressure, J. Rheumatol. 17 (1990) 579–582.
[33] N. Katila, R. Duwa, S. Bhurtel, S. Khanal, S. Maharjan, J.H. Jeong, et al., Enhancement of blood-brain barrier penetration and the neuroprotective effect of resveratrol, J. Contr. Release 346 (2022) 1–19.
[34] A.C. Santos, I. Pereira, M. Pereira-Silva, L. Ferreira, M. Caldas, M. Collado-González, et al., Nanotechnology-based formulations for resveratrol delivery: effects on resveratrol in vivo bioavailability and bioactivity, Colloids Surf. B Biointerfaces 180 (2019) 127–140.
[35] M. Daheshia, J.Q. Yao, The interleukin 1β pathway in the pathogenesis of osteoarthritis, J. Rheumatol. 35 (2008) 2306–2312.
[36] E. Calvo, I. Palacios, E. Delgado, J. Ruiz-Cabello, P. Hernández, O. Sánchez-Pernaute, et al., High-resolution MRI detects cartilage swelling at the early stages of experimental osteoarthritis, Osteoarthritis Cartilage 9 (2001) 463–472.
[37] E. Calvo, I. Palacios, E. Delgado, O. Sánchez-Pernaute, R. Largo, J. Egido, et al., Histopathological correlation of cartilage swelling detected by magnetic resonance imaging in early experimental osteoarthritis, Osteoarthritis Cartilage 12 (2004) 878–886.
[38] P.J. Watson, T.A. Carpenter, L.D. Hall, J.A. Tyler, Cartilage swelling and loss in a spontaneous model of osteoarthritis visualized by magnetic resonance imaging, Osteoarthritis Cartilage 4 (1996) 197–207.
[39] F.W. Roemer, R. Frobell, D.J. Hunter, M.D. Crema, W. Fischer, K. Bohndorf, et al., MRI-detected subchondral bone marrow signal alterations of the knee joint: terminology, imaging appearance, relevance and radiological diferential diagnosis, Osteoarthritis Cartilage 17 (2009) 1115–1131.
[40] J.P. Pelletier, J.P. Raynauld, F. Abram, B. Haraoui, D. Choquette, J. Martel-Pelletier, A new non-invasive method to assess synovitis severity in relation to symptoms and cartilage volume loss in knee osteoarthritis patients using MRI, Osteoarthritis Cartilage 16 (Suppl 3) (2008). S8–13.
[41] D. Loeuille, A.C. Rat, J.C. Goebel, J. Champigneulle, A. Blum, P. Netter, et al., Magnetic resonance imaging in osteoarthritis: which method best refects synovial membrane infammation? Correlations with clinical, macroscopic and microscopic features, Osteoarthritis Cartilage 17 (2009) 1186–1192.
[42] S. Drevet, B. Favier, B. Lardy, G. Gavazzi, E. Brun, New imaging tools for mouse models of osteoarthritis, Geroscience 44 (2022) 639–650.
[43] G.A. Orozco, K. Karjalainen, E.K. Moo, L. Stenroth, P. Tanska, J.L. Rios, et al., A musculoskeletal finite element model of rat knee joint for evaluating cartilage biomechanics during gait, PLoS Comput. Biol. 18 (2022), e1009398.
[44] J.E. Collins, E. Losina, M.C. Nevitt, F.W. Roemer, A. Guermazi, J.A. Lynch, et al., Semiquantitative imaging biomarkers of knee osteoarthritis progression: data from the foundation for the national institutes of health osteoarthritis biomarkers consortium, Arthritis Rheumatol. 68 (2016) 2422–2431.
[45] P.M. Jungmann, F. Liu, T.M. Link, What has imaging contributed to the epidemiological understanding of osteoarthritis? Skeletal Radiol. 43 (2014) 271–275.
[46] M. Banjar, S. Horiuchi, D.N. Gedeon, H. Yoshioka, Review of quantitative knee articular cartilage MR imaging, Magn. Reson. Med. Sci. 21 (2022) 29–40.
[47] W. Waldstein, G. Perino, S.L. Gilbert, S.A. Maher, R. Windhager, F. Boettner, OARSI osteoarthritis cartilage histopathology assessment system: a biomechanical evaluation in the human knee, J. Orthop. Res. 34 (2016) 135–140.
[48] M. Kapoor, J. Martel-Pelletier, D. Lajeunesse, J.P. Pelletier, H. Fahmi, Role of proinflammatory cytokines in the pathophysiology of osteoarthritis, Nat. Rev. Rheumatol. 7 (2011) 33–42.
[49] T. Mabey, S. Honsawek, Cytokines as biochemical markers for knee osteoarthritis, World J. Orthoped. 6 (2015) 95–105.
[50] W.S. Lian, J.Y. Ko, R.W. Wu, Y.C. Sun, Y.S. Chen, S.L. Wu, et al., MicroRNA-128a represses chondrocyte autophagy and exacerbates knee osteoarthritis by disrupting Atg12, Cell Death Dis. 9 (2018) 919.
[51] K.K. Vuppalapati, T. Bouderlique, P.T. Newton, V.O. Kaminskyy, H. Wehtje, C. Ohlsson, et al., Targeted deletion of autophagy genes Atg5 or Atg7 in the chondrocytes promotes caspase-dependent cell death and leads to mild growth retardation, J. Bone Miner. Res. 30 (2015) 2249–2261.
[52] F.J. Blanco, R. Guitian, E. Vázquez-Martul, F.J. de Toro, F. Galdo, Osteoarthritis chondrocytes die by apoptosis. A possible pathway for osteoarthritis pathology, Arthritis Rheum. 41 (1998) 284–289.
[53] Q. Liang, X.P. Wang, T.S. Chen, Resveratrol protects rabbit articular chondrocyte against sodium nitroprusside-induced apoptosis via scavenging ROS, Apoptosis 19 (2014) 1354–1363.
[54] M. Dave, M. Attur, G. Palmer, H.E. Al-Mussawir, L. Kennish, J. Patel, et al., The antioxidant resveratrol protects against chondrocyte apoptosis via effects on mitochondrial polarization and ATP production, Arthritis Rheum. 58 (2008) 2786–2797.
[55] G. Zhang, H. Zhang, W. You, X. Tang, X. Li, Z. Gong, Therapeutic Effect of resveratrol in the treatment of osteoarthritis via the MALAT1/miR-9/NF-κB signaling pathway, Exp. Ther. Med. 19 (2020) 2343–2352.